Nanotechnology Perceptions
ISSN 1660-6795
www.nano-*ntp.com*

Preparation And Characterization Of Copper Oxide And Zinc Oxide Nanoparticles And Evaluation Of Their Anti-Bacterial Activity

Dr. B.B.V. Sailaja[1], Rajesh Tamminana[2]

[1]*Assistant Professor, Department of Chemistry, Andhra University, Visakhapatnam, Andhra Pradesh, India.*
[2]*Research Scholar (Part time), Department of Chemistry, Andhra University, Visakhapatnam, Andhra Pradesh, India.*

Herein, we report on the synthesis of metal oxide nanoparticles (NPs) of copper oxide (CuO) and zinc oxide (ZnO) using the sol-gel method. Characterization of as prepared CuO and ZnO nanoparticles was done by using the techniques such as, UV-visible spectroscopy, X-ray Diffraction (XRD), Dynamic Light Scattering (DLS), scanning electron microscopy (SEM) and Fourier transform infrared spectroscopy (FT-IR). The results indicated that solutes of the copper oxide and zinc oxide nanoparticles contains various functional groups with mean size (hydrodynamic diameter) of 0.9 nm and 1.9 nm and zeta potential of -76.6 mV and -90.4 mV, respectively. This study also investigates the antimicrobial efficacy of copper and zinc oxide nanoparticles against Xanthomonas sp. and Pectobacterium sp. by using the paper disc diffusion method and the evaluated against Bronopol (a commercial antibiotic as check). Results revealed that zinc nanoparticles exhibited highest antimicrobial activity compared to copper nanoparticles at 1000 and 2000 ppm concentrations but less than the Bronopol. However, it is to confirm that zinc oxide nanoparticles exhibits antibacterial activity against Xanthomonas sp. whereas, antibacterial activity was not been observed with copper oxide nanoparticles across the concentrations tested.

Keywords: Metal oxide nanoparticles, , Characterization, CuO, ZnO, Eco-friendly methods.

Introduction

Synthesis of nanomaterials has gained significant interest due to their unique properties and diverse applications in an array of disciplines. Nanoparticles are a form of aggregates of atoms or molecules with dimensions below 100 nm in at least one dimension. With the diameters measuring in the scale of 10^{-9} m, they display distinct chemical, physical, and biological properties. These features have highlighted the importance of application of nanoparticles in an array of fields including engineering, electronics, agriculture, pharmaceuticals, and medicine (Rai and Ingle, 2012; Dar and Soytong, 2013). These particles are modified forms of fundamental elements, resulting from changes to their atomic and molecular characteristics (Wang, 2004; Suchea et al., 2006). Nanoparticles exhibit targeted attributes, including enhanced strength, superior electrical conductivity, and increased chemical reactivity (Nykypanchuk et al., 2008). In agriculture, nanotechnology shows promising results in the

management of insect pests through nanocapsules (Chaudhry et al., 2008; Rai and Ingle, 2012). Applying silicon to susceptible wheat cultivars has enhanced crop resistance and reduced pest invasions and developing nanostructured catalysts may also improve pesticide efficacy, potentially allowing for reduced dosages (Basagli et al., 2003; Moraes et al., 2004; El-bendary and El-Helaly, 2013).

Despite being having handful of available methods, sol-gel process provides advantages over other methods, like, low-temperature material production and controlled nanoparticle synthesis, enhancing efficacy and stability. By adjusting temperature, pH, and concentration, researchers can optimize nanoparticle size and morphology, influencing biological interactions (Radhakrishnan and Benna, 2014). In agriculture, metal oxides like copper oxide and zinc oxide show promise in plant nutrition and pest management by improving nutrient absorption and enhancing plant resistance to pathogens consequently increasing yields while minimizing chemical use. In medicine, nanoparticles are recognized for their biocompatibility and specific targeting capabilities, enabling innovative therapeutic approaches, including drug delivery systems and antimicrobial agents. Notably, bacterial nanocellulose has shown significant potential in biomedical applications, underscoring the versatility of nanomaterials in both fields (Fernandes et al., 2023).

It has been reported that nanoparticles of ZnO and CuO exhibits higher bio-efficacy as compared to that of bulk size (Riyadh et al., 2015). Zinc is a necessary element to our health and ZnO nano particles additionally have right biocompatibility with human cells [He et al., 2011]. Recently ZnO and CuO are listed as safe material by FDA (food and drug administration, (USA) (Emamifar et al., 2010). Further, both copper oxide (CuO) and zinc oxide (ZnO) have shown varying antibacterial activity in opposition to micro- organism species. However, the anti-microbial activities of these nano-substances should be thoroughly evaluated against gram positive and gram negative bacteria species (Asamoah et al.,2020). This study explores cost-effective, environmental friendly methods for large-scale production of CuO and ZnO nanoparticles via the sol-gel technique and also examines their efficacy in combating plant pathogens like, Xanthomonas sp. and Pectobacterium sp., which extrapolates their implications for sustainable agriculture.

Material and methods

2.1 Synthesis of metal oxide nanoparticles (CuO and ZnO)

All chemicals were procured of analytical grade. Copper (II) nitrate trihydrate and zinc acetate dihydrate were used as precursors, with sodium citrate tri-basic dehydrate as the precipitating reagent. All chemicals were obtained from Sigma Aldrich, and aqueous solutions were prepared with deionized water from MilliQ (Milli-Q Water Systems, USA). Metal oxide nanoparticles were synthesized using a simple wet chemical precipitation method, which converts ionic solutions into insoluble nanometal oxide precipitates. Pure crystalline nanometal oxides are obtained by separating the precipitates, drying, and calcination.

2.1.1 Synthesis of copper oxide (CuO) nanoparticles:

Nanoscale CuO particles were synthesized via the sol-gel method, mixing 1% copper (II) nitrate tetrahydrate with 0.05% sodium citrate tribasic dehydrate. The solution was stirred at 700 rpm and 60 °C for 2 hours, and then the pH was adjusted to 11 with 2 M NaOH, followed by one more hour of stirring. A black suspension formed, indicating copper oxide production (Kumar et al., 2013; Asamoah et al., 2020). After cooling to room temperature, precipitates were separated by centrifugation and washed with distilled water. The particles were dried at 80 °C overnight and calcined at 600 °C for 6 hours to remove impurities.

2.1.2 Synthesis of zinc oxide (ZnO) nanoparticles

Oxalate decomposition technique was used to prepare ZnO-nanoparticulates. In brief, equimolar (0.2 M) solutions of zinc acetate and oxalic acid mixed to prepare zinc oxalate. The aqueous solutions stirred for about 12 h. The white precipitate so formed as a result of mixing zinc acetate and oxalic acid was collected by filtration and thoroughly washed with double de-ionized water (DI-water) and allowed to dry in the air at room temperature. Then the oxalate made into fine powder form and decomposed in the air by keeping it in a pre-heated muffle furnace for 45 minutes at 500°C.

2.2 Characterization of metal oxide nanoparticles of CuO and ZnO

Nanoparticle properties are influenced by synthesis methods and parameters. This study characterized their crystal structure, elemental composition, optical properties, morphology, and functional groups using UV-Vis spectroscopy, Fourier transform infrared spectroscopy, X-ray diffraction, dynamic light scattering and transmission electron microscopy.

2.2.1 UV–Vis spectroscopic analysis

The UV–visible absorbance spectrum represents the characteristic absorbance of a given material. Many molecules absorb ultraviolet or visible light and the intensity of absorption (A) or optical density (O.D) was recorded as a function of wavelength. The UV-visible spectra of the test solution were recorded in Spectrophotometer UV-2600i (SHIMADZU).

2.2.2 FT-IR (Fourier transform infrared spectroscopy) analysis

FT-IR is a powerful tool for isolating and characterizing organic contamination. When infrared rays are passed through a sample, some of the radiation is absorbed by the sample and some is transmitted. FTIR measures the absorption of infrared radiation by the sample material versus wavelength. FTIR is particularly useful for the identification of organic molecular groups and compounds all of which have the characteristic vibration frequencies in the infrared range. The FTIR spectrum was taken in the mid-IR region of 400–4000 cm^{-1}. The spectrum was recorded using the ATR (attenuated total reflectance) technique. The dried sample was mixed with the KBr (1:200) crystal, and the spectrum was recorded in the transmittance mode (Tensor 27, BRUKER).

2.2.3 X-ray diffraction (XRD) analysis

XRD is a crystallographic technique used for determining the atomic and molecular structure of a crystal (for understanding material properties), in which the crystalline atoms cause a beam of incident X-rays to diffract into many specific directions. A focused x-ray beam is shot at the sample at a specific angle of incidence. X-ray diffraction (XRD) analysis was performed

on a Diffractometer (SHIMADZU, XRD700) using Cu Kα radiation for all analyses at 40 kV and 30mA to identify the phases of the powders. The crystal size of the nanoscale powder was calculated with the Scherer formula from data of FWHM of the XRD spectrum. The XRD patterns were recorded in the 2 range = 30–80° using a step size of 0.02° and a counting time of 5 seconds per step.

2.2.4 Particle size and zeta potential analysis

Particle size and zeta potential can be determined by measuring the random changes in the intensity of light scattered from a suspension or solution. This technique is known as dynamic light scattering (DLS). But is also called photon correlation spectroscopy (PCS) and quasi-elastic light scattering (QELS). It works based on the principle of Brownian motion and Doppler shift. Zeta potential is a key indicator of the stability of colloidal dispersions. The aqueous suspension of the synthesized nanoparticles was filtered through a 0.22 μm syringe filter unit and the size of the distributed nanoparticles was measured by using the principle of Dynamic Light Scattering (DLS) technique made in a Nanopartica (HORIBA, SZ-100) compact scattering spectrometer.

2.2.5 Study of particle morphology (SEM)

Scanning electron microscope (SEM) creates various images by focusing a high-energy beam of electrons onto the surface of a sample and detecting signals from the interaction of the incident electron with the sample's surface. SEM images have a greater depth of field yielding a characteristic 3D appearance useful for understanding the morphology of the material. Samples were observed under a scanning electron microscope at magnification ranging from 10X to 600,000X operated at an accelerating voltage of 30 kV.

2.3 Antibacterial testing

Evaluation of the antibacterial activity of the prepared nanometal oxides were performed under sterile conditions in a laminar flow cabinet. All culture media, pipette tips, water, and glassware were sterilized by autoclaving at 121 °C for 15 minutes. Xanthomonas citri pv. citri (XCC) and Pectobacterium carotovorum were used in the studies. The cultures obtained from Department of Plant Pathology, Citrus Research Staiton, Petluru, Dr YSR Horticultural University, Andhra Pradesh, India - 524132

2.3.1. Agar diffusion tests

Agar diffusion tests were performed using the Kirby-Bauer method. CuO and ZnO stock solutions were prepared at the concentrations of 1000 ppm and 2000 ppm. Sterile 5 mm filter paper disks were dipped into each aqueous suspension of nanoparticles and allowed to soak completely. Subsequently, nutrient agar (NA) media was prepared by dissolving 0.5% peptone, 0.1% beef extract, 0.2 % yeast extract, 0.5% sodium chloride and 1.5% agar in one litre of deionised water. The solution was autoclaved for 15 min at 121°C. Petri plates of about 9 cm diameter were filled with the prepared NA in a sterilized laminar flow chamber and allowed to solidify shortly. A suspension of Xanthomonas citri pv. citri (XCC) and Pectobacterium carotovorum were introduced into separate conical flasks containing molten media prior to plating. The filter paper disks were placed on the agar plate using sterilised forceps. The plates

were incubated at 37°C overnight. Zone of inhibition around filter disks, due to antibacterial activity of the nanoparticles, observed and measured. Bronopol was used as the control.

3.0 RESULTS AND DISCUSSION

3.1 Synthesis of oxide nanoparticles of Cu and Zn

The nanoparticles chosen for this study, specifically copper (Cu) and zinc (Zn), were synthesised utilising the sol-gel method, with minor modifications. This approach was selected due to its advantages, including ease of synthesis, low-temperature decomposition, and the ability to control the chemical composition. The sol-gel method is a highly effective technique for the synthesis of copper oxide (CuO) and zinc oxide (ZnO) nanoparticles and this method facilitates precise control over particle size and distribution. The sol-gel method is particularly notable for its versatility and control, involving the hydrolysis and condensation of precursors to form a gel, which is subsequently dried and thermally treated to yield nanoparticles. This approach ensures uniform particle size and a high surface area, thereby improving efficacy in agricultural applications. Furthermore, its cost-effectiveness and scalability render it suitable for large-scale production (Fernandes et al., 2023; Gopalakrishnan et al., 2016).

3.2 Characterization of nanoparticles

The synthesized nanoparticles were characterized for absorbance, presence of functional groups, size, zeta potential and structure, and the results obtained regarding characterization were given below. The XRD results were discussed and interpreted as per JCPDS card (2020) given by International Centre for Diffraction Data (ICDD).

3.2.1 UV-Visible Spectroscopy study

The UV–Vis spectrum of nanoscale metal oxides of zinc and copper showed absorption peaks within the range of 200 nm to approximately 400 nm (De Caro and Haller, 2025). A UV–Vis analysis of the synthesised copper oxide and zinc oxide nanoparticles is shown in Fig. 1 and 2. The ultraviolet-visible (UV-Vis) spectrum depicting absorbance (Abs.) as a function of wavelength exhibited the characteristic absorption peak for copper was identified at 275 nm, indicating that the conversion of copper ions to copper oxide nanoparticles reached its maximum at this wavelength, indicative of an electron transition from the valence band to the conduction band. This suggests a significant conversion of Cu^{2+} ions to metallic copper nanoparticles, resulting in an increased concentration of copper nanoparticles. This phenomenon is attributed to the transition from the 2p orbital of oxygen to the 4s orbital of Cu^{2+} (Dahrul and Alatas, 2016). The extensive range of the spectrum, spanning from ultraviolet (UV) to visible light, is characteristic of nanometal oxides. Notably, the highest peak is observed in the UV region (Mondal, 2017). Additionally, it was observed that the intensity of the surface plasmon absorption peak extended up to 280 nm over time, during which the rate of reduction of copper ions to copper oxide nanoparticles exhibited a gradual decline. The broad spectral range also suggests that the nanoparticles possess a variety of sizes and shapes (Khashan et al., 2018).

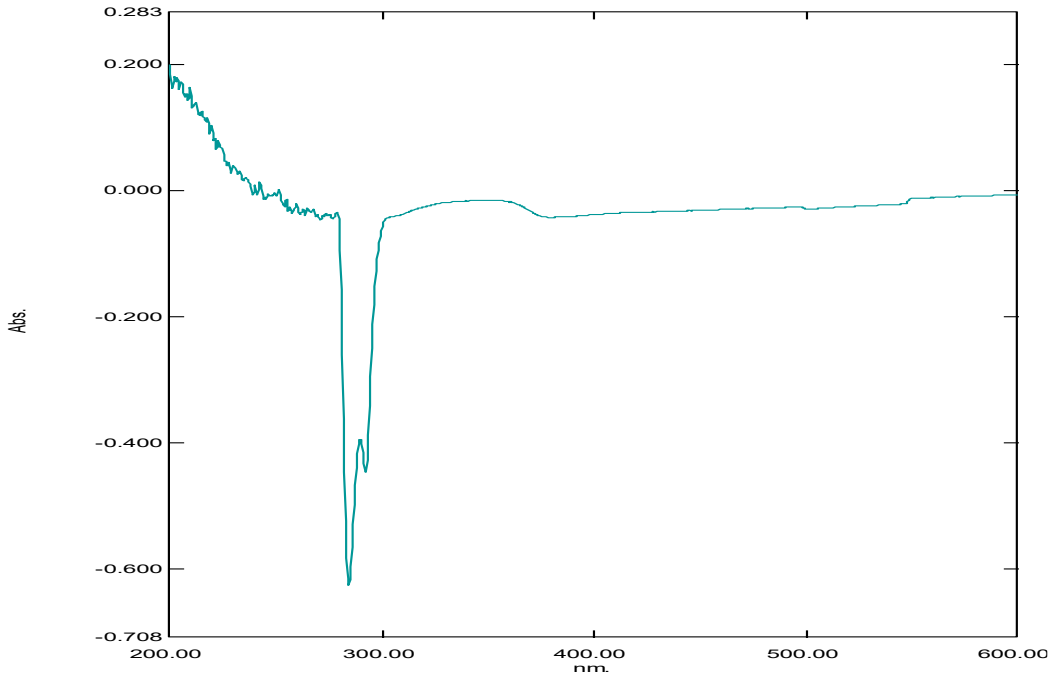

Figure 1: UV–Vis spectrophotometer of Copper Oxide showing peak absorbance

Zinc oxide nanoparticles show a sharp peak at 270 nm where the oscillation of the conducting electrons was initiated (Fig. 2). This is due to the electron transfer across its band-gap. Electron transition occurs between the valence band and its conduction band. The 2d oxygen band is the valence band of ZnO while the 3d orbital of Zn^{2+} is the conduction band (Kumar et al., 2013). The peak was attained at 270 nm indicating the maximum presence of zinc nanoparticles in the reaction mixture at that point. Their initial peak further rose due to oscillation of more electrons after five hours which depicted the continuous synthesis of zinc nanoparticles for a prolonged period.

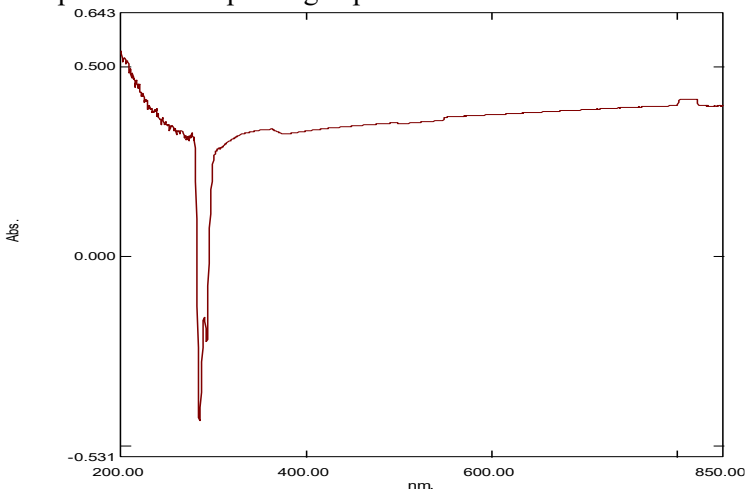

Figure 2. UV–Vis spectrophotometer of Zinc Oxide showing peak absorbance

3.2.2 FTIR (Fourier transform infrared spectroscopy) analysis

FT-IR spectroscopy analysis was done to identify the functional groups that are present in the hydrosols of zinc oxide and copper oxide nanoparticles. The Infrared absorption band identifies the presence of various functional groups in the hydrosols. Both synthesized nano-particles CuO and ZnO have been scanned from 4000 to 400 cm^{-1}. The region from 4000 to 1500 cm^{-1} was the functional group region and region from 1500 to 667 cm^{-1} was the fingerprint region (Arunraja et al., 2016).

The infrared spectra of copper oxide nanoparticles was shown in Fig. 3. The peaks observed at 593, 479 and 411cm^{-1} are the bands associated with the stretching vibrations of Cu–O bonds, revealed formation of copper oxide. The absorption bands within 1350 cm^{-1} and 1650 cm^{-1} are the indications of atmospheric CO_2 and bands are not formed in this range. Spectra bands occurring between 2800 and 3500 cm^{-1} correspond to O–H bonds. O–H bonds with no bands are due to the absence of moisture content. The graph indicated that the peaks present at 2654 and 2034 cm^{-1} indicated the -C≡C- stretching vibration of alkynes, 1087 and 1018 cm^{-1} indicated the C-H way stretching vibration of alkyl halides and 822 cm^{-1} indicated the C-Cl stretching vibration of alkyl halides. The FTIR in Fig.3 confirms that copper oxide was synthesised and confirmed by the presence of Cu–O bond (Renuga et al 2020).

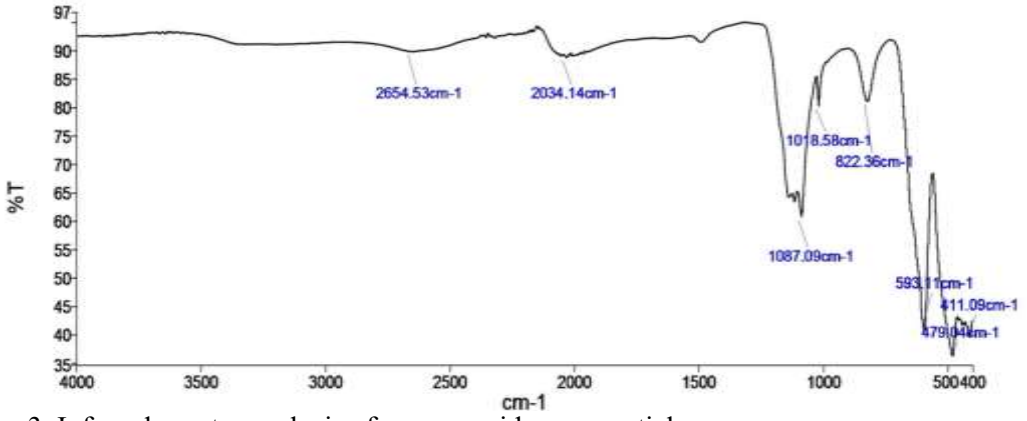

Fig. 3. Infrared spectra analysis of copper oxide nanoparticles.

The FTIR spectrum of ZnO NPs was observed at 3693, 3648, 3444, 1480, 1418, 1119, 885, 853, 796, 590 and 427 cm^{-1} (Fig. 4). The peak obtained at 427 cm^{-1} could be attributed to zinc and oxygen bonding vibrations. This peak corresponds to previous study findings (Nimbalkar and Patil, 2017). The peaks observed at 3693 3648 and 3444 cm^{-1} could be appointed to hydroxyl (OH) groups, 1480 and 1418 cm^{-1} correspond to aliphatic C–H stretching vibrations. A deep absorbance band at 1119 indicates the presence of carbohydrate (C–O), (C═C) rings. The FTIR in Fig. 3 confirms that copper oxide was synthesised and confirmed by the presence of Cu–O bond. The FTIR spectra analysis of zinc oxide is shown in Fig. 4. The absorption band at 427 cm^{-1} is an indication of Zn–O vibration. The FTIR spectra show that there was surfactant present on the surface of both nanoparticle samples. These peaks are These peaks correspond to previous study findings (Renuga et al 2020, Nimbalkar and Patil, 2017 and Faisal, et al., 2021)

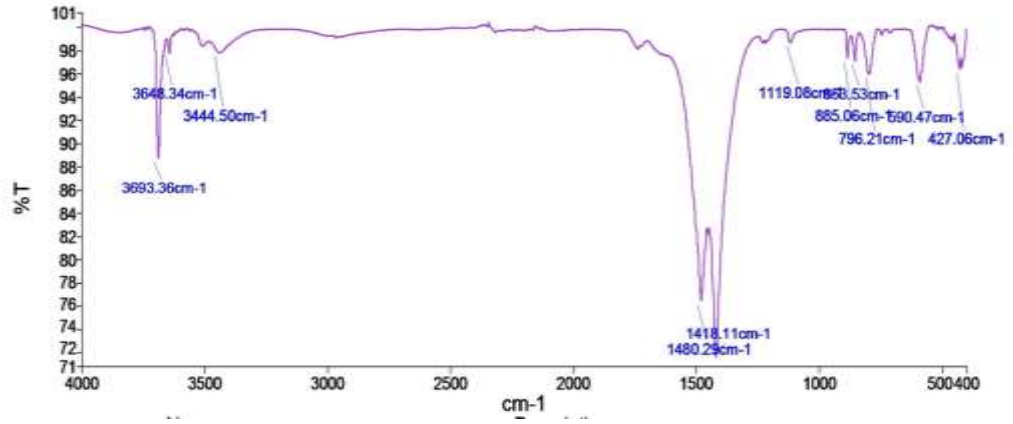

Fig. 4. Infrared spectra analysis of zinc oxide nanoparticles.

3.2.3 X-Ray diffraction (XRD) analysis

The XRD patterns reveal that the synthesised nanometal oxides were fine and free of impurities. The peak positions (figure 5) with 2θ values of 32.5°, 35.6°, 38.7°, 48.9°, 58.3°, 66.4°, 68.1°, 72.5° and 75.1° can be assigned to the planes (−111), (002), (111), (−202), (202), (−311), (113), (311) and (400) which corresponds to monoclinic phase of Copper oxide (JCPDS card no 45-0937) (Abboud et al., 2014). The average particle size D is estimated using Debye–Scherrer equation by determining the width of (−111) peak. These phases were indexed to the cubic shape of the nanoparticles. The diffraction patterns demonstrate sharp peaks as indication of the good crystallinity of the nano powders. The XRD patterns obtained for copper oxide are in exact agreement with the monoclinic phase of copper oxide (Ref). The spectra peaks had a precise correlation with that of the monoclinic phase.

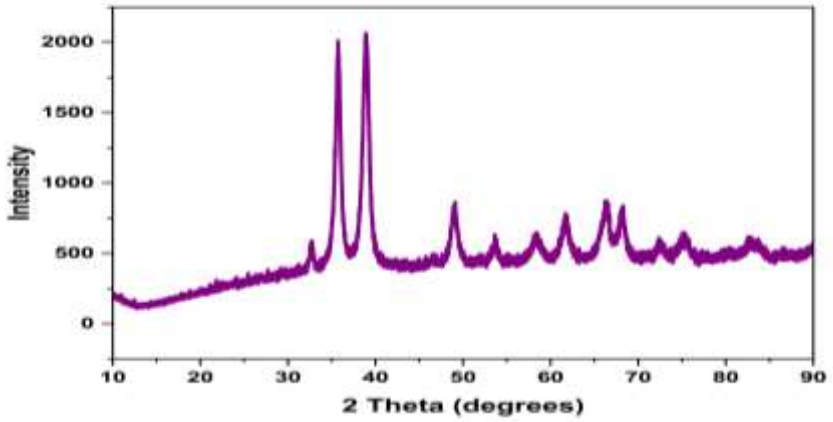

Fig. 5 shows the XRD spectra pattern for copper oxide

The X-ray diffraction pattern of zinc oxide nanoparticles shows definite line broadening of the X-ray diffraction peaks, showing that the prepared particles were in the nanoscale range, as shown in Figure 6. The diffraction peaks located at 31.5, 34.4, 36.2, 47.5, 56.4, 62.8, and 67.9° have been indexed as the spherical to the hexagonal phase of ZnO with high crystallinity (Zhou

et al., 2007 and Khoshhesab et al 2011) with (JCPDS card number 36-1451). It was revealed that all of the characteristic peaks were of ZnO-NPs, and the composition was free from impurities. The diameter of zinc oxide crystallites was calculated by the Debye–Scherrer formula. On the bases of θ (Bragg's diffraction angle) and β (full width at half-maximum (FWHM)) of more intense peaks corresponding to 101 planes located at position 36.2°, the crystallite size is about 29 nm, (Kaskow et al 2018) while the average crystallite size is 41.23 nm. The indexation confirms the standard hexagonal wurtzite structure (JCPDS file no. 00-036-1451) of ZnO-NPs, as previously reported in other studies (Arakha et al., 2015). No peaks due to impurity were observed, which suggests the high purity of zinc oxide obtained. In addition, the peak was widened implying that the particle size is very small, indicating the crystallinity of the synthesized solids. Traditionally, the broadening of the peaks in the XRD patterns of solids is attributed to particle size effects.

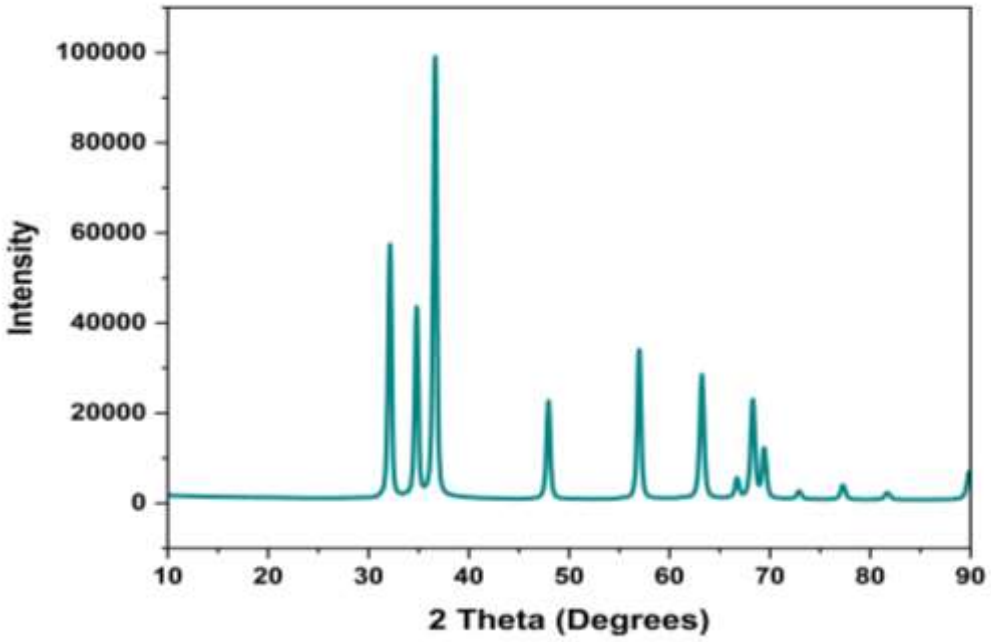

Fig. 6 shows the XRD spectra pattern for zinc oxide.

3.2.4 Dynamic light scattering (DLS) analysis

The size distribution and ζ-potential of the CuO-NPs were investigated using the dynamic light scattering (DLS) technique. The ζ-potential defines the colloidal stability and is a typical measurement of the surface charge on a particle. Particle size determination of the formulated copper nanoparticles was shown under different categories like size distribution by dynamic light scattering and stability by zeta potential. The results presented in Figure 7 indicated that the particle size for the copper nanoparticles was 0.9 nm. The zeta potential was -76.6mV and the electrophoretic mobility mean was -0.000594 cm^2/vs.

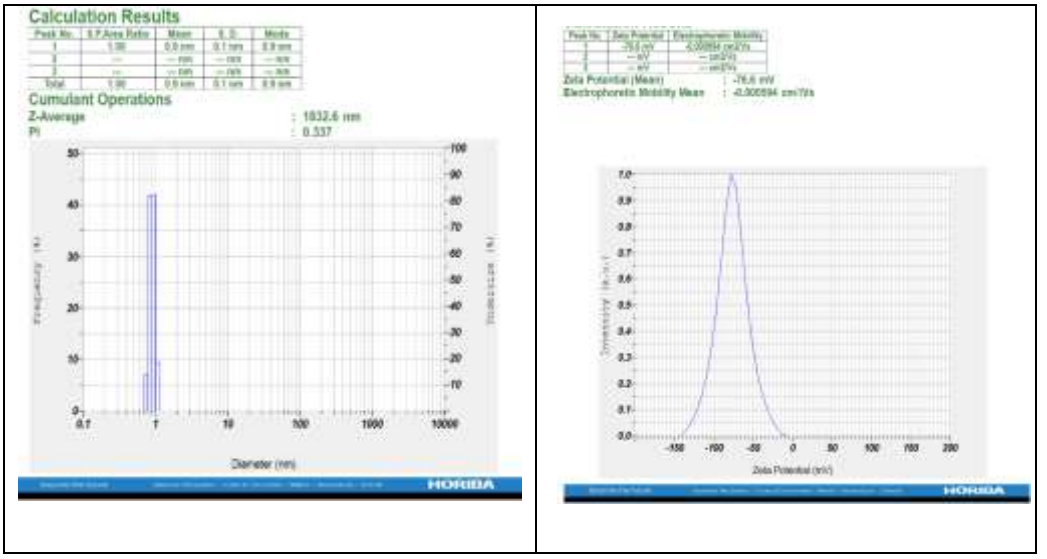

Figure 7. (A) Size distribution potential and (B) ζ-potential distributionCuO-NPs.

The size distribution and ζ-potential of the synthesized ZnO-NPs were investigated using the dynamic light scattering (DLS) technique resented in Figure 8 revealed that the particle size recorded for the zinc nanoparticles was 1.9 nm with a zeta potential of -90.4 mV while the electrophoretic mobility mean was 0.000701cm^2/vs

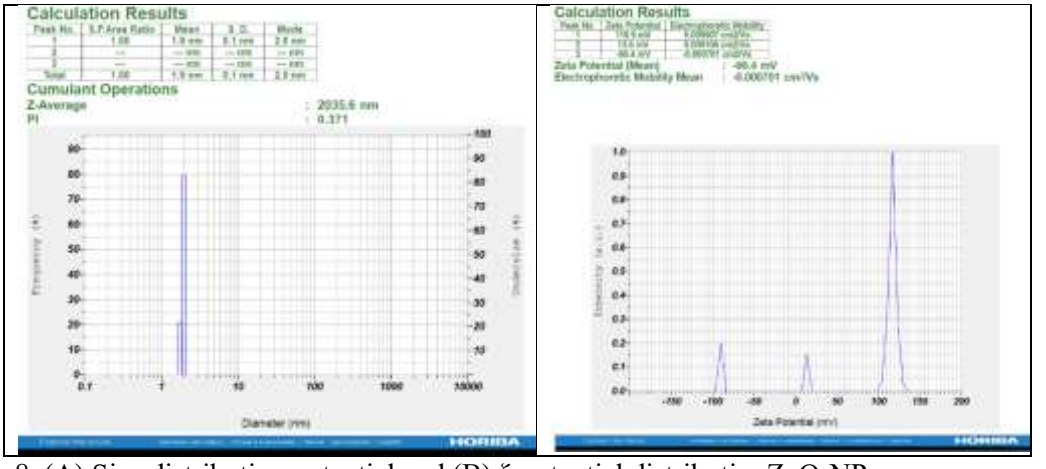

Figure 8. (A) Size distribution potential and (B) ζ-potential distributionZnO-NPs.

3.2.5 Scanning electron microscopy (SEM)

Morphology of CuO and ZnO Particles synthesized by sol–gel method and the size of the formed CuO and ZnO nano- particles have been studied by SEM technique at

different magnification shown in Figs.9 and 10 respectively. Scanning electron microscopy images show similar appearance for the presence of copper nanoparticles and synthesized nanoparticles were in 200 nm range.

The SEM image shows cluster of nanoparticles with slight agglomeration. Irregular flower petals like shapes have been observed in the micrographs.

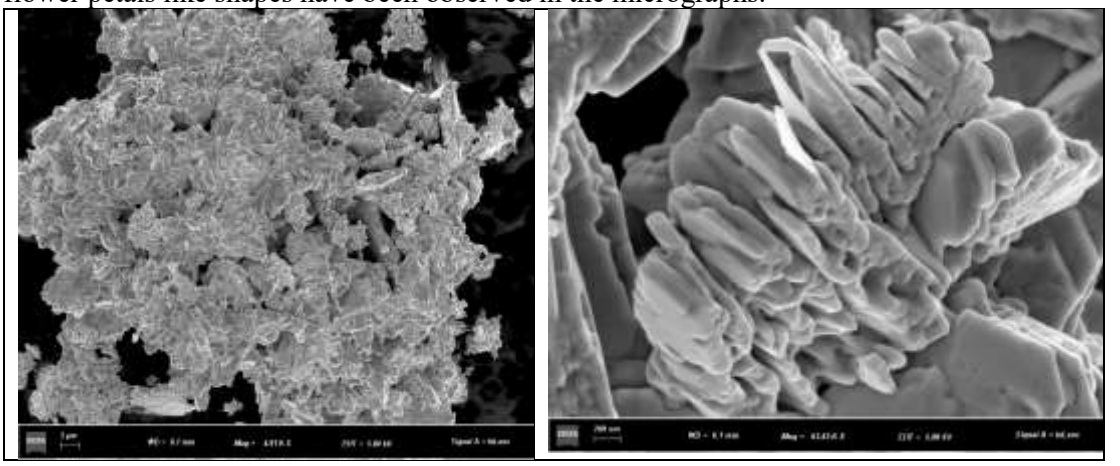

Fig. 9 Scanning electron microscopy micrograph of CuO NPs.

The morphological study of the sol gel synthesized zinc oxide nanoparticles was performed by Scanning electron microscopy. The particles show a cluster of nanoparticles with slight agglomeration and the shape of the nanoparticle was spherical to semispherical shape, and these particles are as shown in Figure 10. This clearly shows that the particles are present in a homogeneous form and the homogeneity of nanoparticles plays important roles in their different activities. The particle size ranged from 30 to 100 nm. The size increase was due to the overlapping of particles on each other. SEM studies confirmed the presence of zinc nanoparticle.

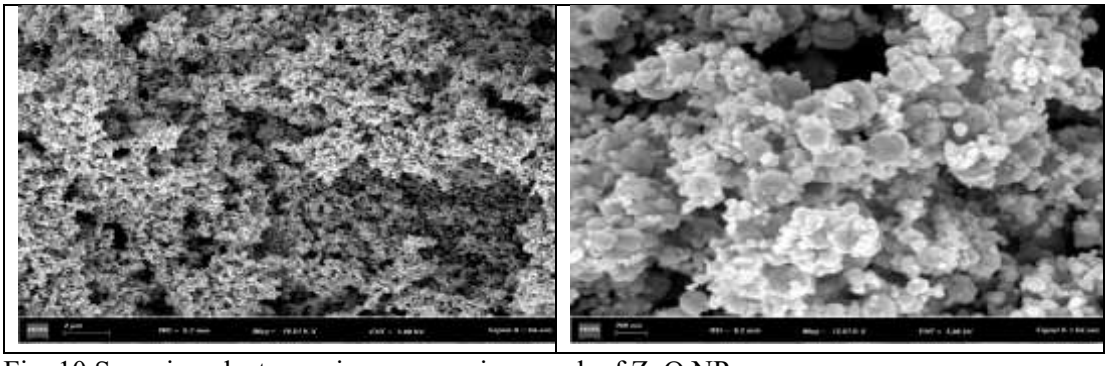

Fig. 10 Scanning electron microscopy micrograph of ZnO NPs.

3.3 Antibacterial activity

The antibacterial activity of CuO and ZnO nanoparticles was examined against both Xanthomonas citri pv. citri and Pectobacterium carotovorum by using disc diffusion test. The radial diameter of the inhibition zone of bacteria presented in Figure 11 and 12. In the current study, it was observed that 1000 and 2000 ppm CuO-NP solution not display any anti-microbial activity against Xanthomonas citri pv. citri and Pectobacterium carotovorum. On the other hand, 1000 and 2000 ppm ZnO-NP solution displayed maximum zone of inhibition against Xanthomonas citri pv. citri (26.55±1.85) but not observe any anti-microbial activity against Pectobacterium carotovorum (Table. 1)

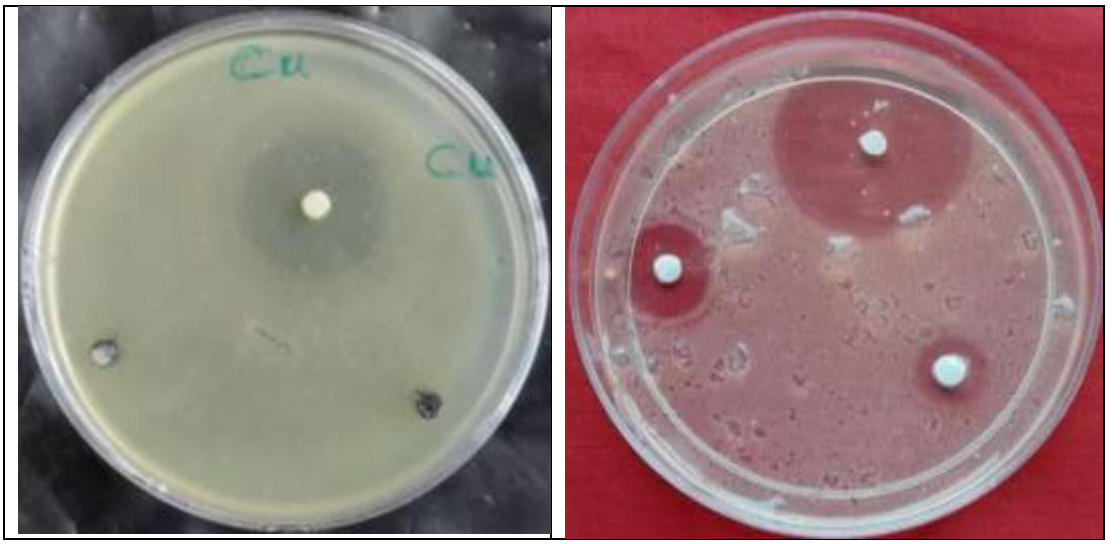

Fig 11 Antibacterial assay with CuO and ZnO nanoparticles zone of inhibition against Xanthomonas citri pv. citri (XCC).

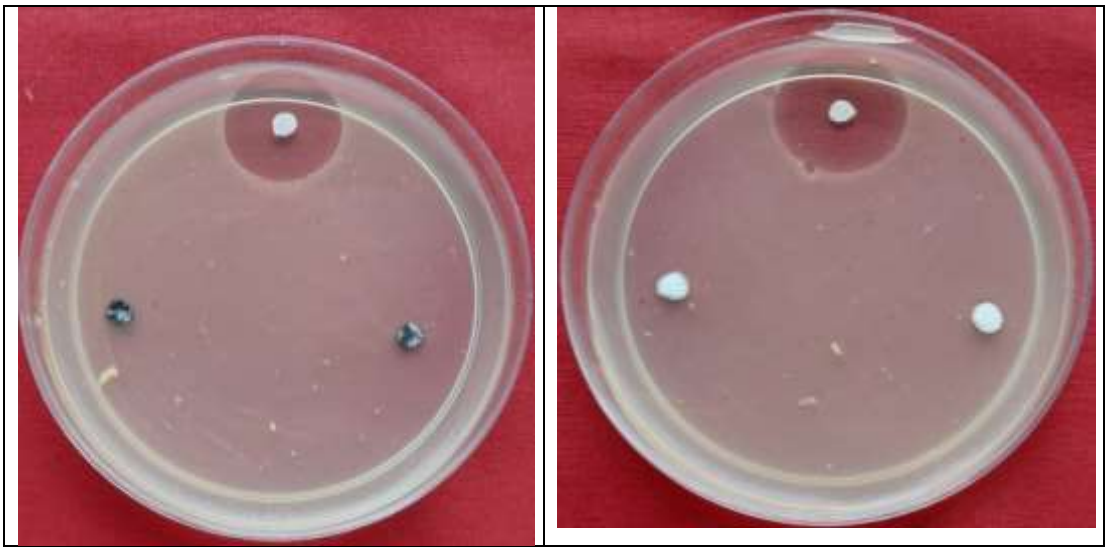

Fig 12 Antibacterial assay with CuO and ZnO nanoparticles zone of inhibition against

Pectobacterium carotovorum

Table 1. Antibacterial Activity of CuO and ZnO-NPs against Xanthomonas citri pv. citri and Pectobacterium carotovorum

Nanoarticles	Concentration (ppm)	Inhibition zone (mm± sd)	
		Xanthomonas citri pv. citri	Pectobacterium carotovorum
CuO -NPs	1000	0.00	0.00
	2000	0.00	0.00
ZnO-NPs	1000	11.35±1.40	0.00
	2000	26.55±1.85	0.00
Control (Bronopal)	500	38.85±1.15	19.65±0.80

Conclusion: In the present work, we report a convenient method for the synthesis of CuO and ZnO nanoparticles using the sol-gel method. The developed nanoparticles were characterized by UV–Vis, SEM, XRD, Zeta potential and FTIR measurements. Further, nano ZnO particles exhibited good antibacterial activity whereas; nano CuO particles are not effective against the species tested. This sol gel technique can be a promising method for preparing other metal oxide nanoparticles which can be potential applications in agriculture, environmental, pharmaceutical and medical applications.

Acknowledgement:
The authors heartily acknowledge the Department of Chemistry, Andhra University, Visakhapatnam, Andhra Pradesh, India, for supporting this work.

Literature cited

1. Abboud, Y., Saffaj, T., Chagraoui, A. El Bouari, A. Brouzi, K.. Tanane, O and Ihssane, B. Biosynthesis, characterization and antimicrobial activity of copper oxide nanoparticles (CONPs) produced using brown alga extract (Bifurcaria bifurcata). Appl Nanosci **4**, 571–576 (2014). https://doi.org/10.1007/s13204-013-0233-x
2. Arakha, M., Saleem, M., Mallick, B. C. and Jha, S. The effects of interfacial potential on antimicrobial propensity of ZnO nanoparticle, Sci Rep., **5**, 9578 (2015). https://doi.org/10.1038/srep09578
3. Arunraja, L., Thirumoorthy, P., Karthik, A., Sriram, G., Rajendran, V. and Edwinpaul, L. Structural and Electrical Properties of Cadmium Sulfide Nanoparticles: A Simple Chemical Route, Synthesis and Reactivity in Inorganic Metal-Organic and Nano-Metal Chemistry, 46 (11), 1642-1646 (2016). https://doi.org/10.1080/15533174.2015.1137037.
4. Asamoah, R. B., Yaya, A., Mensah, B., Nbalayim, P., Apalangya, V., Bensah, Y. D., Damoah, L.N.W., Agyei-Tuffour, B., Dodoo-Arhin, D. and Annan, E. Synthesis and characterization of zinc and copper oxide nanoparticles and their antibacteria activity, Results in Materials, 7,100099 (2020). https://doi.org/10.1016/j.rinma.2020.100099.
5. Basagli, M. A. B., Moraes, J. C., Carvalho, G. A., Ecole, C. C. and De, C. R. R. Effect of sodium silicate application on the resistance of wheat plants to the green aphid Schizaphis graminum (Rond.) (Hemiptera: Aphididae). Neotrop. Entomol., 32 (4), 659-663 (2003). https://doi.org/10.1590/S1519-566X2003000400017
6. Chaudhry, Q., Scotter, M., Blackburn, J., Ross, B., Boxall, A., Castle, L., Aitken, R. and Watkins, R. Applications and implications of nanotechnologies for the food sector, Food Addit Contam Part A Chem Anal Control Expo Risk Assess., 25(3), 241-258 (2008). https://doi.org/10.1080/02652030701744538
7. Dahrul, M. and Alatas, H. Preparation and optical properties study of CuO thin film as applied solar cell on LAPAN-IPB Satellite. Procedia Environmental Sciences, 33, 661-667(2016). https://doi.org/10.1016/j.proenv.2016.03.121

8. Dar, J. and Soytong, K. Engineering organic nanoparticle as delivery system of bio-active compounds from Chaetomium spp. for plant disease control; C2013.
9. De Caro, C. A. and Haller, C. UV/VIS Spectrophotometry—Fundamentals and Applications. Mettler-Toledo Publication No. ME-30256131 (2025).
10. Moraes, J. C., Goussain, M. M., Basagli, M. A. B., Carvalho, G. A., Ecole, C. C. and Sampaio, M. V. Silicon influence on the tritophic interaction: wheat pests, the greenbug Schizaphis graminum (Rondani) (Hemiptera: Aphididae), and its natural enemies, Chrysoperla externa (Hagen) (Neuroptera: Chrysopidae) and Aphidius colemani Viereck (Hymenoptera: Aphididae). Neotrop. Entomol., 33 (5), 619-624 (2004). http://dx.doi.org/10.1590/S1519-566X2004000500012
11. El-bendary, H. M. and El-Helaly, A. A. First record nanotechnology in agricultural: Silica nanoparticles a potential new insecticide for pest control. App. Sci. Report. 4 (3), 241-246 (2013).
12. Emamifar, A., Kadivar, M., Shahedi, M., and Soleimanian-Zad, S. Evaluation of nanocomposite packaging containing Ag and ZnO on shelf life of fresh orange juice. Innovative Food Science & Emerging Technologies, 11(4), 742-748 (2010). http://dx.doi.org/10.1016/j.ifset.2010.06.003
13. Faisal Shah, Hasnain Jan, Sajjad Ali Shah, Sumaira Shah, Adnan Khan, Muhammad Taj Akbar, Muhammad Rizwan, Faheem Jan,, Noreen Akhtar, Aishma Khattak, and Suliman Syed. Green Synthesis of Zinc Oxide (ZnO) Nanoparticles Using Aqueous Fruit Extracts of Myristica fragrans: Their Characterizations and Biological and Environmental Applications ACS Omega 2021 6 (14), 9709-9722 (2021). https://doi.org/10.1021/acsomega.1c00310
14. Fernandes M., González-Ballesteros N., da Costa A., Machado R., Gomes A. C. and Rodríguez-Argüelles M. C. Antimicrobial and anti-biofilm activity of silver nanoparticles biosynthesized with Cystoseira algae extracts. J Biol Inorg Chem **28**, 439–450 (2023). https://doi.org/10.1007/s00775-023-01999-y
15. Gopalakrishnan, L., Doriya, K., Santhosh, D. Moringa oleifera: a review on nutritive importance and its medicinal application Food Sci. Hum. Wellness, 5 49-56 (2016). https://doi.org/10.1016/j.fshw.2016.04.001
16. He, H., Yang, Q., Wang, J., and Ye, Z. Layer-structured ZnO nanowire arrays with dominant surface-and acceptor-related emissions. Materials Letters, 65(9), 1351-1354 (2011). http://dx.doi.org/10.1016/j.matlet.2011.01.080
17. Karthik, K. V., Raghu, A. V., Reddy, K. R., Ravishankar, R., Sangeeta, M., Shetti, N. P. and Reddy, C. V. Green synthesis of Cu-doped ZnO nanoparticles and its application for the photocatalytic degradation of hazardous organic pollutants. Chemosphere, 287 (2), 132081 (2022). http://dx.doi.org/10.1016/j.chemosphere.2021.132081
18. Kaskow, I. Decyk, P. and Sobczak, I. The effect of copper and silver on the properties of Au-ZnO catalyst and its activity in glycerol oxidation. Appl. Surf. Sci., 444, 197– 207 (2018). https://doi.org/10.1016/j.apsusc.2018.02.285
19. Khashan, K. S., Jabir, M. S., and Abdulameer, F. A. Preparation and characterization of copper oxide nanoparticles decorated carbon nanoparticles using laser ablation in liquid. In Journal of Physics: Conference Series 1003, 012100 (2018). http://dx.doi.org/10.1088/1742-6596/1003/1/012100
20. Khoshhesab, Z. M., Sarfaraz, M., and Asadabad, M. A. Preparation of ZnO Nanostructures by Chemical Precipitation Method. Synthesis and Reactivity in Inorganic, Metal-Organic, and Nano-Metal Chemistry, 41(7), 814–819 (2011).
21. https://doi.org/10.1080/15533174.2011.591308
22. Kumar, A., Saxena, A., De, A., Shankar, R., & Mozumdar, S. Facile synthesis of size-tunable copper and copper oxide nanoparticles using reverse microemulsions. Rsc Advances, 3(15), 5015-5021 (2013). https://doi.org/10.1039/C3RA23455J
23. Suchea, M., Christoulakis, S., Moschovis, K., Katsarakis, N. and Kiriakids, G. ZnO ransparent thin films for gas sensor applications, Thin solid films 515 (2), 551-554 (2006). https://doi.org/10.1016/j.tsf.2005.12.295
24. Mondal, K. Recent advances in the synthesis of metal oxide nanofibers and their environmental remediation applications. Inventions, 2 (2), 9 (2017).
25. https://doi.org/10.3390/inventions2020009
26. Nimbalkar, A. R. and Patil, M. G. Synthesis of ZnO thin film by sol-gel spin coating technique for H_2S gas sensing application. Physica B, 527, 7–15 (2017).
27. https://doi.org/10.1016/j.physb.2017.09.112
28. Nykypanchuk, D., Maye, M., van der Lelie, D. and Gang, Oleg. DNA-guided crystallization of colloidal nanoparticles. Nature 451 (7178), 549–552 (2008).

29. https://doi.org/10.1038/nature06560
30. Radhakrishnan, A. A., and Beena, B. B. Structural and optical absorption analysis of CuO nanoparticles. Indian J. Adv. Chem. Sci, 2(2), 158-161 (2014).
31. Rai, M. and Ingle, A. Role of Nanotechnology in Agriculture with Special Reference to Management of Insect Pests. Applied Microbiology and Biotechnology, 94 (2), 287-293 (2012). https://doi.org/10.1007/s00253-012-3969-4
32. Renuga, D., Jeyasundari, J., Shakthi Athithan, A. S., Brightson Arul Jacob, Y. Synthesis and characterization of copper oxide nanoparticles using Brassica oleracea var. italic extract for its antifungal application. Mater. Res. Express, 7 (04), 5007 (2020). http://dx.doi.org/10.1088/2053-1591/ab7b94
33. Riyadh, M. A., Quraish, A. K., Kassim, M. S., Rawaa, A. A., Roaa, J. M., Noor, A. and Kand Alwan, N. J. Synthesis of zinc oxide nanoparticles via sol-gel route and their characterization. Nano Sci Nanotech., 5 (1) 1-6, (2015). doi: 10.5923/j.nn.20150501.01
34. Sriram, G., Bendre, A., Altalhi, T., Jung, H. Y., Hegde, G. and Kurkuri, M. Surface engineering of silica based materials with Ni–Fe layered double hydroxide for the efficient removal of methyl orange: Isotherms, kinetics, mechanism and high selectivity studies. Chemosphere, 287(Pt 1), 131976 (2022).
35. http://dx.doi.org/10.1016/j.chemosphere.2021.131976
36. Sriram, G., Dhineshbabu, N. R., Nithyavathy, N., Saminathan, K., Kaler, K. V. I. S. and Rajendran, V. Sensitivity and response of polyvinyl alcohol/tin oxide nanocomposite multilayer thin film sensors. Journal of Nanoscience and Nanotechnology, 16(1), 1008-1017 (2016). http://dx.doi.org/10.1166/jnn.2016.10669
37. Zhong Lin Wang. Zinc oxide nanostructures: growth, properties and Application. Journal of Physics: Condensed Matter, 16(25), 829-858 (2004). http://dx.doi.org/10.1088/0953-8984/16/25/R01
38. Zhou, J., Zhao, F., Wang, Y., Zhang, Y. and Yang, L. Size-controlled synthesis of ZnO nanoparticles and their photoluminescence properties. J. Lumin., 122 (1), 195– 197 (2007). http://dx.doi.org/10.1016/j.jlumin.2006.01.089